Isotropic-nematic transition in an external field

Juelian Shen and Chia-Wei Woo
*Department of Physics, University of California, San Diego, La Jolla, California 92093**
and Institute of Physics, Chinese Academy of Sciences, Beijing, China†
(Received 13 January 1981)

We study the effects of an external field on the isotropic-nematic transition in liquid-crystalline substances. The theoretical technique employed is called the "orientationally averaged pair correlations" approximation. It takes into detailed account spatial correlations between the molecules while treating orientational order in a mean-field-like manner. The results obtained for MBBA (4-methoxybenzylidene-4′-*n*-butylaniline) are compared to those of the Maier-Saupe theory and the Landau–de Gennes theory. We determine the paranematic-nematic coexistence curve, the temperature-external field phase diagram, the Cotton-Mouton coefficient, the maximum supercooling temperature, critical exponents, and the relation between the transition temperature and the electric field in laser-induced isotropic-nematic transitions. These results are compared to experimental data. Their implications are discussed.

I. INTRODUCTION

We present in this paper a molecular-theoretic calculation of the effect of an external aligning field on the isotropic-nematic transition in liquid-crystalline substances.

The external field considered can be a magnetic field, on a system with a (positive) molecular diamagnetic anisotropy, $(\Delta\chi)_{max} = \chi_{\parallel} - \chi_{\perp}$. The variation of the induced orientational order parameter σ_2, with the square of the field H^2, gives rise to what is known as the Cotton-Mouton coefficient. The latter's temperature dependence in turn gives us a model-dependent estimate of the maximum supercooling temperature,[1-4] T^*. A plot of its fractional increase over its zero-field value with respect to the temperature enables one to examine the critical behavior of the system[4] in the region $T \gtrsim T^*$. Moreover, by plotting $\sigma_2(T)$ at varying H, one can obtain the paranematic-nematic coexistence curve and a T-H phase diagram, and identify a critical point (T_{PN}^c, H_c) at which the transition ceases to be first order in nature.

The external field can also be an electric field, as provided for by pulses from an intense laser beam. At temperatures close to the zero-field clearing temperature $T_{IN} \equiv T_{PN}(0)$, a transition from the isotropic to the nematic phase can be induced,[6-8] which may ultimately be exploited for practical applications.

As far as we know, theoretical work on I-N transitions under the influence of an external electromagnetic field has been limited to mean-field approximations, either in the phenomenological Landau–de Gennes formulation[1-4] or in the molecular-theoretic Maier-Saupe formulation.[5] In our group, we have attempted to improve theoretical contacts with experiment in both phenomenological and molecular-theoretic directions. In the former, we concentrate on going beyond the Gaussian approximation, i.e., including the cubic and quartic terms of the free energy in the treatment of fluctuations, and on the consideration of volume dependences of the free energy. Some progress has been made, and will be reported elsewhere.[9] In the latter, we have concentrated on improving the model by taking into account anisotropic steric effects,[10,11] and going beyond the usual mean-field approximation by considering spatial correlations between the molecules.[12-17] We feel that our theoretical apparatus is now sufficiently reliable[17] to warrant a quantitative calculation for the isotropic-nematic transition in an external aligning field.

Section II outlines our theoretical formalism, known as the "orientationally averaged pair correlations" approximation (OAPC). It shows how the inclusion of spatial correlation effects extends the mean-field theory to a somewhat complicated double self-consistency scheme which is, nevertheless, amenable to mathematical solution. We also give a method for evaluating the free energy without truncating a cluster series for the entropy. Section III displays our numerical results for MBBA (4-methoxybenzylidene-4′-*n*-butylaniline). The physical quantities and the phase diagram obtained are compared to those of the mean-field calculations. Section IV interprets these results, first for an external magnetic field, and next for an electric field. We conclude with a few remarks on the experimental implications of our theory.

II. THEORETICAL FORMALISM

The theoretical formalism outlined here turns out to be very similar to that in Ref. 17, al-

though there is no *a priori* reason to expect it to remain so clean, now that an external field has been added.

We consider a system of N cylindrically symmetric molecules in a volume $\mathcal{V}$, so that the number density is given by $\rho \equiv N/\mathcal{V}$. The molecules interact via a nonchiral, pairwise potential

$$v_{ij} \equiv v(\vec{r}_i, \hat{\Omega}_i, \vec{r}_j, \hat{\Omega}_j) \equiv v(r_{ij}, \hat{\Omega}_i \cdot \hat{\Omega}_j, \hat{\Omega}_i \cdot \hat{r}_{ij}, \hat{\Omega}_j \cdot \hat{r}_{ij})$$
$$= v_0(r_{ij}) + v_2(r_{ij}) P_2(\hat{\Omega}_i \cdot \hat{\Omega}_j) + v_4(r_{ij}) P_4(\hat{\Omega}_i \cdot \hat{\Omega}_j), \tag{1}$$

where $\vec{r}_i$ and $\hat{\Omega}_i$ denote the position and orientation of the ith molecule, and P_2 and P_4 are Legendre polynomials. The model represented by Eq. (1) is far from general. It results from a truncated expansion, and lacks dependences on $\hat{\Omega}_i \cdot \hat{r}_{ij}$ and $\hat{\Omega}_j \cdot \hat{r}_{ij}$, which would have brought forth important anisotropic steric effects. But it stands for the best that one can do in the present state of the art. (See, nevertheless, Refs. 10 and 11.)

The potential energy of the system is given by

$$V = \sum_{\substack{i<j \\ =1}}^{N} v_{ij} + \sum_{i=1}^{N} \nu P_2(\cos\theta_i), \tag{2}$$

where $\cos\theta_i$ denotes $\hat{\Omega}_i \cdot \hat{n}$, $\hat{n}$ being the director, and ν embodies a susceptibility to the external field. In particular, for a molecule in a magnetic field H,

$$\nu = \frac{-(\Delta\chi)_{\max} H^2}{3}. \tag{3}$$

The molecular theory begins with the Helmholtz free-energy functional

$$\mathfrak{F}\{P_N(1,\ldots,N)\} = F_0 + \int V \frac{P_N(1,\ldots,N)}{N!}\, d1 \cdots dN + kT \int \frac{P_N(1,\ldots,N)}{N!} \ln \frac{P_N(1,\ldots,N)}{N!}\, d1 \cdots dN, \tag{4}$$

where $P_N(1,\ldots,N)$ stands for the N-particle distribution function normalized as follows:

$$\int P_N(1,\ldots,N)\, d1 \cdots dN = N!, \tag{5}$$

and di denotes $d\vec{r}_i d\hat{\Omega}_i$. As was observed in Ref. 17, a direct minimization of $\mathfrak{F}$ with respect to P_N would lead to an equilibrium distribution which is simply the Boltzmann distribution function, as expected.

To render the free energy computationally tractable, we must apply simplifying approximations to P_N. The mean-field approximation arises if P_N assumes the form of a single-particle product: $P_N(1,\ldots,N) \approx N! \prod_{i=1}^{N} Q(\hat{\Omega}_i)$. For systems as dense as liquid crystals, one must introduce at least *some* degree of spatial correlations. Thus in the "orientationally averaged pair correlations" approximation (OAPC) one assumes

$$P_N(1,\ldots,N) \approx N! \prod_{i=1}^{N} Q(\hat{\Omega}_i) \cdot \phi_N(\vec{r}_1,\ldots,\vec{r}_N), \tag{6}$$

with Q and ϕ_N separately normalized to satisfy Eq. (5), thus:

$$\int Q(\hat{\Omega})\, d\hat{\Omega} = 1, \tag{7}$$

and

$$\int \phi_N(\vec{r}_1,\ldots,\vec{r}_N)\, d\vec{r}_1 \cdots d\vec{r}_N = 1. \tag{8}$$

The reason for naming this approximation OAPC will become obvious presently.

Substituting Eq. (6) into the expression (4) for $\mathfrak{F}$ yields

$$\mathfrak{F}\{P_N(1,\ldots,N)\} \equiv \mathfrak{F}\{Q(\hat{\Omega}), \phi_N(\vec{r}_1,\ldots,\vec{r}_N)\} = F_0 + \sum_{\substack{i<j \\ =1}}^{N} \int \bar{v}_{ij}\, \phi_N(\vec{r}_1,\ldots,\vec{r}_N)\, d\vec{r}_1 \cdots d\vec{r}_N$$
$$+ \sum_{i=1}^{N} \int \nu P_2(\cos\theta_i) Q(\hat{\Omega}_i)\, d\hat{\Omega}_i + kT \sum_{i=1}^{N} \int Q(\hat{\Omega}_i) \ln Q(\hat{\Omega}_i)\, d\hat{\Omega}_i$$
$$+ kT \int \phi_N(\vec{r}_1,\ldots,\vec{r}_N) \ln \phi_N(\vec{r}_1,\ldots,\vec{r}_N)\, d\vec{r}_1 \cdots d\vec{r}_N, \tag{9}$$

where

$$\bar{v}_{ij} \equiv \int v_{ij} Q(\hat{\Omega}_i) Q(\hat{\Omega}_j)\, d\hat{\Omega}_i d\hat{\Omega}_j \tag{10}$$

plays the natural role of an orientationally averaged pair potential.

Minimizing $\mathfrak{F}$ with respect to Q and ϕ_N, taking into account the normalization conditions (7) and (8) by including Lagrange multiplier terms with $\mathfrak{F}$, leads to

$$Q(\hat{\Omega}_i) = Z_\Omega^{-1} \exp\left[-\frac{1}{kT}\left(\sum_{j(\neq i)} \int v_{ij} Q(\hat{\Omega}_j)\phi_N(\vec{r}_1, \ldots, \vec{r}_N) d\hat{\Omega}_j d\vec{r}_1 \cdots d\vec{r}_N + \nu P_2(\cos\theta_i)\right)\right], \tag{11}$$

with

$$Z_\Omega = \int \exp\left[-\frac{1}{kT}\left(\sum_{j(\neq i)} \int v_{ij} Q(\hat{\Omega}_j)\phi_N(\vec{r}_1, \ldots, \vec{r}_N) d\hat{\Omega}_j d\vec{r}_1 \cdots d\vec{r}_N + \nu P_2(\cos\theta_i)\right)\right] d\hat{\Omega}_i, \tag{12}$$

and

$$\phi_N(\vec{r}_1, \ldots, \vec{r}_N) = Z_r^{-1} \exp\left(-\frac{1}{kT}\sum_{i<j} \bar{v}_{ij}\right), \tag{13}$$

with

$$Z_r = \int \exp\left(-\frac{1}{kT}\sum_{i<j} \bar{v}_{ij}\right) d\vec{r}_1 \cdots d\vec{r}_N. \tag{14}$$

These results when substituted back into Eq. (9) gives rise to a free energy expression:

$$F = F_0 - NkT \ln Z_\Omega - kT \ln Z_r - \sum_{\substack{i \neq j \\ =1}}^{N} \int \bar{v}_{ij}\, \phi_N(\vec{r}_1, \ldots, \vec{r}_N) d\vec{r}_1 \cdots d\vec{r}_N. \tag{15}$$

Note that even though Eq. (15) looks exactly like Eq. (20) in Ref. 17, $Q(\Omega)$ is now different. There will be orientational order even when the temperature exceeds the zero-field transition temperature T_{IN}. The order comes, first of all, from the external field aligning each molecule individually. Since $Q(\hat{\Omega})$ enters $\phi_N(\vec{r}_1, \ldots, \vec{r}_N)$ through $\bar{v}_{ij}$, as defined in Eq. (10), there will be many-body correlation effects in Z_Ω, Z_r, $\bar{v}_{ij}$, and ϕ_N. As a result the free energy F will be profoundly different from that of Ref. 17. It is now a function of ρ, T, and the strength of the external field. The two quasiequilibrium phases, obtained from solving the double self-consistent equations (10)–(14), will now include a weakly ordered phase that replaces the isotropic phase, and a strongly ordered phase, which is a slightly modified nematic phase. The weakly ordered phase is called "paranematic" for obvious reasons.

Only one more step remains before we call forth an explicit form of the model potential. $\phi_N(\vec{r}_1, \ldots, \vec{r}_N)$ appears in the form of a Boltzmann distribution function for a classical fluid of particles interacting via an effective potential $\bar{v}_{ij}$. One can therefore define n-particle distribution functions in the usual manner:

$$\phi_n(\vec{r}_1, \ldots, \vec{r}_n) = \frac{N!}{(N-n)!} \int \phi_N(\vec{r}_1, \ldots, \vec{r}_N) d\vec{r}_{n+1} \cdots d\vec{r}_N. \tag{16}$$

In particular, *for a central* $\bar{v}_{ij}$,

$$\phi_2(\vec{r}_1, \vec{r}_2) \equiv \phi_2(r_{12}) = \frac{N(N-1)}{Z_r} \int \exp\left(\frac{-1}{kT}\sum_{i<j} \bar{v}_{ij}\right) d\vec{r}_3 \cdots d\vec{r}_N \equiv \rho^2 g(r_{12}), \tag{17}$$

and

$$\phi_3(\vec{r}_1, \vec{r}_2, \vec{r}_3) \equiv \phi_3(r_{12}, r_{23}, r_{31}) = \frac{N(N-1)(N-2)}{Z_r} \int \exp\left(\frac{-1}{kT}\sum_{i<j} \bar{v}_{ij}\right) d\vec{r}_4 \cdots d\vec{r}_N$$

$$\equiv \rho^3 g_3(r_{12}, r_{23}, r_{31}) \approx \rho^3 g(r_{12}) g(r_{23}) g(r_{31}). \tag{18}$$

The last step of Eq. (18) states the well known closure relation called the Kirkwood superposition approximation (KSA). $g(r)$ can be solved from an equation obtained by differentiating its definition (17) and using Eq. (18) in the resulting expression, the so-called BBGKY equation (Bogoliubov-Born-Green-Kirkwood-Yvon):

$$\nabla_1 \ln g(r_{12}) = -\frac{1}{kT}\nabla_1 \bar{v}_{12} - \frac{\rho}{kT} \int g(r_{23}) g(r_{31}) \nabla_1 \bar{v}_{13} d\vec{r}_3. \tag{19}$$

We are now ready to turn toward applying the above formalism to our specific model, Eq. (1). Recognizing that for uniaxiality

$$Q(\hat{\Omega}) = \frac{1}{2\pi} Q(\theta), \tag{20}$$

we obtain with the definition given in Eq. (10):

$$\bar{v}_{ij} = v_0(r_{ij}) + v_2(r_{ij})\sigma_2^2 + v_4(r_{ij})\sigma_4^2, \tag{21}$$

where

$$\sigma_{2l} = \int Q(\hat{\Omega}) P_{2l}(\cos\theta) d\hat{\Omega} = \int Q(\theta) P_{2l}(\cos\theta) \sin\theta d\theta, \quad l = 1, 2. \tag{22}$$

And from Eqs. (11) and (12),

$$Q(\hat{\Omega}) \equiv \frac{1}{2\pi} Q(\theta) = Z_\Omega^{-1} \exp\left(\frac{-1}{kT} [\rho\gamma_0 + \rho\gamma_2\sigma_2 P_2(\cos\theta) + \rho\gamma_4\sigma_4 P_4(\cos\theta) + \nu P_2(\cos\theta)]\right), \tag{23}$$

with

$$Z_\Omega = \int \exp\left(\frac{-1}{kT} [\rho\gamma_0 + \rho\gamma_2\sigma_2 P_2(\cos\theta) + \rho\gamma_4\sigma_4 P_4(\cos\theta) + \nu P_2(\cos\theta)]\right) d\hat{\Omega}, \tag{24}$$

and

$$\gamma_{2l} = \int v_{2l}(r) g(r) d\vec{r}, \quad l = 0, 1, 2. \tag{25}$$

Defining a new normalization constant:

$$Z_\theta = [2\pi \exp(-\rho\gamma_0/kT)]^{-1} Z_\Omega = \int \exp\left(\frac{-1}{kT} [(\rho\gamma_2\sigma_2 + \nu) P_2(\cos\theta) + \rho\gamma_4\sigma_4 P_4(\cos\theta)]\right) \sin\theta d\theta, \tag{26}$$

we obtain

$$Q(\theta) = Z_\theta^{-1} \exp\left(\frac{-1}{kT} [(\rho\gamma_2\sigma_2 + \nu) P_2(\cos\theta) + \rho\gamma_4\sigma_4 P_4(\cos\theta)]\right), \tag{27}$$

and subsequently from Eqs. (15)–(17), (21), and (25),

$$F = F_0 - NkT \ln 2\pi - NkT \ln Z_\theta - kT \ln Z_r - N\rho\gamma_2\sigma_2^2 - N\rho\gamma_4\sigma_4^2. \tag{28}$$

Finally, from the definition of Z_r in Eq. (14), we find

$$\frac{\partial \ln Z_r}{\partial \sigma_{2l}^2} = \frac{-1}{2kT} N\rho\gamma_{2l}, \quad l = 1, 2. \tag{29}$$

Thus,

$$\ln Z_r = -\frac{N\rho}{2kT} \sum_{l=1}^{2} \int \gamma_{2l} d\sigma_{2l}^2. \tag{30}$$

Absorbing the constants of integration into $(F_0 - NkT \ln 2\pi)$, Eq. (28) now reads:

$$F = F_0' - NkT \ln Z_\theta + \tfrac{1}{2} N\rho \int_0^{\sigma_2^2} \gamma_2(\sigma_2^2, \sigma_4^2) d\sigma_2^2 + \tfrac{1}{2} N\rho \int_0^{\sigma_4^2} \gamma_4(\sigma_2^2, \sigma_4^2) d\sigma_4^2 - N\rho\gamma_2\sigma_2^2 - N\rho\gamma_4\sigma_4^2. \tag{31}$$

This completes our theoretical derivations. The procedure of calculation will be summarized in the next section.

III. PROCEDURE AND RESULTS OF CALCULATION

Equations (11) and (13), or their reduced version, Equations (27) and (19), form a pair of coupled equations which describe both orientational and spatial ordering. Equation (27) contains the moments γ_{2l}, which through Eq. (25) depend on $g(r)$. It also contains σ_{2l}, which through Eq. (22) depend self-consistently on $Q(\theta)$. Equations (19)–(22) and (26)–(27) form the basis of a double self-consistency scheme.

Beginning with, e.g., the mean-field solution and its corresponding order parameters σ_{2l}^{MF}, we can use Eq. (21) to evaluate the orientationally averaged pair potential $\bar{v}_{ij}$. Equation (19) then gives us $g(r)$. From Eq. (25), we calculate the interaction strengths γ_{2l}, which when entered into Eq. (27) produce a new set of order parameters with the help of the self-consistent equation (22). This set of order parameters can now be used to start a new cycle of calculation. The calculation continues in this iterative fashion until the output agrees with the input σ_{2l}. That completes the second nest of the self-consistency.

Such calculations are to be performed for a given set of model parameters in the potential (1), and for every set of the thermodynamic variables (ρ, T, ν). In each case, after the solution or solutions have been determined, they are used in Eqs. (26) and (31) to obtain the free energies. The stable phase corresponds to the solution that minimizes the free energy. (In principle, a Maxwell construction should be carried out to

take into account the volume change that occurs in a first-order transition even though the volume changes are quite small for isotropic-nematic transitions.)

Our actual computational algorithm is somewhat different from that described above. We search directly for self-consistent solutions in the (σ_2^2, σ_4^2) space. After finding the solutions, we evaluate γ_{2l} along straight-line paths from the origin (0, 0) to each solution (σ_2^2, σ_4^2), and perform the integrations in Eq. (31) along these paths. Our procedure will, of course, lead to the same results as an iterative process, but after acquiring some experience we can get to the solutions much faster. The solution of the integro-differential equation (19) is very costly. It is crucial to select judiciously the correct regions in the (σ_2^2, σ_4^2) space in our search for the solutions, rather than letting an iterative process direct us in the search.

For MBBA, we take the potential of Ref. 17, i.e.,

$$v_0(r) = 4\epsilon_0\left[\left(\frac{a_0}{r}\right)^{12} - \left(\frac{a_0}{r}\right)^{6}\right],$$

$$v_2(r) = -4\epsilon_2\left(\frac{a_2}{r}\right)^{6}, \tag{32}$$

$$v_4(r) = -4\epsilon_4\left(\frac{a_4}{r}\right)^{6},$$

with $a_0 = a_2 = a_4 = 6.655$ Å, $\epsilon_0 = 118.35$ kK, $\epsilon_2 = 78.90$ kK, and $\epsilon_4 = -55.23$ kK. The values of these parameters were chosen to closely approximate the experimental clearing temperature and orientational order parameter σ_2. (Actually the parameters were chosen such that T_{IN} *at constant density*, which is what one obtains in a calculation that minimizes F, equals approximately 317 K, since we know from experiment and our previous work[13,14] that such a transition temperature lies approximately one degree below the clearing point, which is the transition temperature at constant pressure: about 318 K.) We fix the density at 0.002 315 Å^{-3}, the experimental value of MBBA at clearing, and vary the temperature T and the external field variable ν.

Table I displays our numerical results. The variable $-\nu/kT$ is dimensionless. The paranematic phase refers to the lower branch of the solutions of the double self-consistency, while the nematic phase refers to the upper branch. The transition temperature T_{PN} at $\rho = 0.002\,315$ Å^{-3} refers to the temperature at which paranematic and nematic phases coexist, i.e., when the Helmholtz free energies corresponding to the two branches coincide. At zero field, the paranematic phase is, of course, isotropic, and thus $T_{PN}(0) \equiv T_{IN}$ by definition. (The zero-field results are not exactly identical to those given in Ref. 17 since we have written new computer codes which allow us to examine the numerical output in finer details and higher accuracy. All results are shifted, however, in the same direction. The changes are unimportant.)

In Table II, we select for display some of the intermediate details of the calculation, for the convenience of readers who may wish to repeat or extend our work. It shows two ways of identifying the transition. In the top part of the table, we fixed $-\nu/kT$ at 0.0060 and varied T. The final column identified the transition as taking place at $F_P = F_N$, or 319.4 K. In the lower part of the table, we fixed T at 325.5 K and varied $-\nu/kT$. Interpolation of the numbers that appear in the last column indicated that the transition takes place at about $-\nu/kT = 0.0193$. A more detailed look into that region then determined

TABLE I. Transition temperatures and order parameters in an external field.

$-\nu/kT$	T_{PN} (K) at $\rho = 0.002\,315$ Å^{-3}	Paranematic σ_2	Paranematic σ_2	Nematic σ_2	Nematic σ_4	$T_{PN}(\nu) - T_{PN}(0) \equiv T_{PN}(\nu) - T_{IN}$ (K)
0.0000	316.74	0.000	0.000 00	0.335	0.052	0.00
0.0030	318.06	0.008	0.000 04	0.325	0.049	1.32
0.0040	318.50	0.011	0.000 07	0.322	0.048	1.76
0.0050	318.95	0.014	0.000 10	0.319	0.047	2.21
0.0060	319.40	0.018	0.000 15	0.316	0.046	2.66
0.0070	319.86	0.021	0.000 21	0.313	0.045	3.12
0.0080	320.31	0.024	0.000 30	0.310	0.044	3.57
0.0090	320.77	0.028	0.000 40	0.305	0.043	4.03
0.0100	321.22	0.032	0.000 51	0.300	0.042	4.48
0.0150	325.50	0.051	0.001 30	0.282	0.037	6.76
0.0192	325.50	0.071	0.002 60	0.260	0.031	8.76
0.0246	328.00	0.107	0.006 00	0.226	0.024	11.26
0.0289	330.00	0.165	0.013 00	0.171	0.014	13.26

Table II. Selected intermediate details in our numerical work.

		Paranematic			Nematic			
$-\nu/kT$	T(K)	σ_2	σ_4	$F_P - F_0'$(k K/N)	σ_2	σ_4	$F_N - F_0$(k K/N)	$F_P - F_N$ (k K/N)
0.0060	317.4	0.019 60	0.000 19	−0.017	0.342	0.054	−0.481	0.464
	318.4	0.018 60	0.000 17	−0.017	0.329	0.050	−0.239	0.222
	319.4	0.017 66	0.000 15	−0.016	0.316	0.046	−0.016	0.000
	320.4	0.017 00	0.000 13	−0.015	0.302	0.042	0.187	−0.202
	321.4	0.016 16	0.000 12	−0.015	0.271	0.034	0.363	−0.378
0.0180	325.5	0.062	0.002 0	−0.144	0.245	0.028	−0.062	−0.082
0.0190		0.069	0.002 3	−0.165	0.258	0.031	−0.145	−0.020
0.0195		0.073	0.003 0	−0.177	0.262	0.032	−0.188	+0.011

$-\nu/kT$ exactly at 0.0192, as indicated in Table I. The advantage of the latter method is that, for a given model potential and a chosen set of (σ_2^2, σ_4^2), Eq. (19) is density and temperature dependent, *but not dependent on* ν. Since solving Eq. (19) constitutes the most costly and repeated part of our numerical calculation, sharing it among a spectrum of ν values results in significant savings of computer time.

Figure 1 shows both branches of the order parameter σ_2 at transition as a function of T_{PN}. As a phase diagram, one considers $\sigma_2(T)$ descending toward a point (marked by a cross) on the upper branch of the curve as temperature increases. At that point, it drops discontinuously to a point (marked by a circle) on the lower branch. After which it continues to descend asymptotically toward zero. The solid curve shown in the figure is then the coexistence curve. The numbers along the curve at indicated points represents $-\nu/kT$ values. The cross and the circle at each T_{PN} correspond as a pair with the same $-\nu/kT$. The dashed curve was obtained by Wojtowicz and Sheng[5] using the Maier-Saupe theory and scaled by us to MBBA temperatures. Note that each curve is symmetrical about a horizontal axis. At T_{PN} = 330.1 K, a critical point with σ_2 = 0.168 appears in our case, beyond which the two phases merge and the first-order transition disappears. The Maier-Saupe critical point is higher.

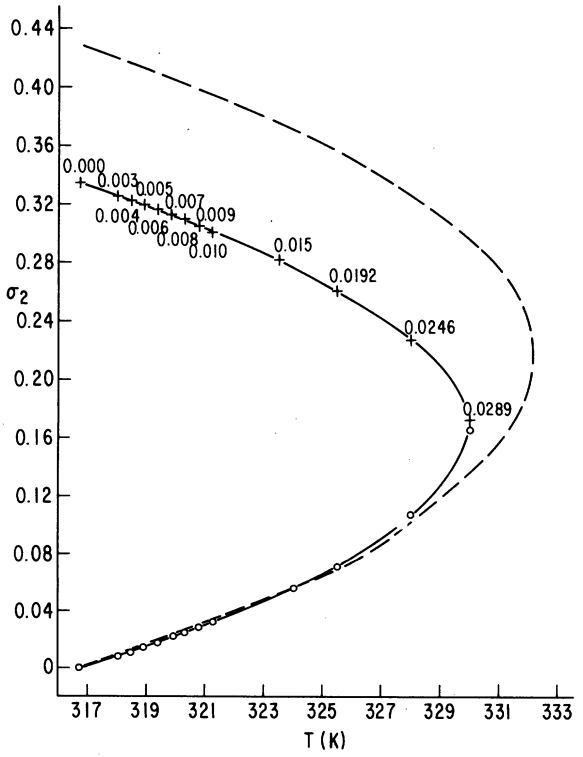

FIG. 1. Coexistence curve: σ_2 at transition temperatures T_{PN}. The flags refer to values of $-\nu/kT$ for pairs of σ_2 in coexisting paranematic (circles) and nematic (crosses) phases. Solid curve: present calculation. Dashed curve: Ref. 5.

Figure 2 shows both branches of the order parameter σ_4 as a function of T_{PN}. Note that σ_4 is

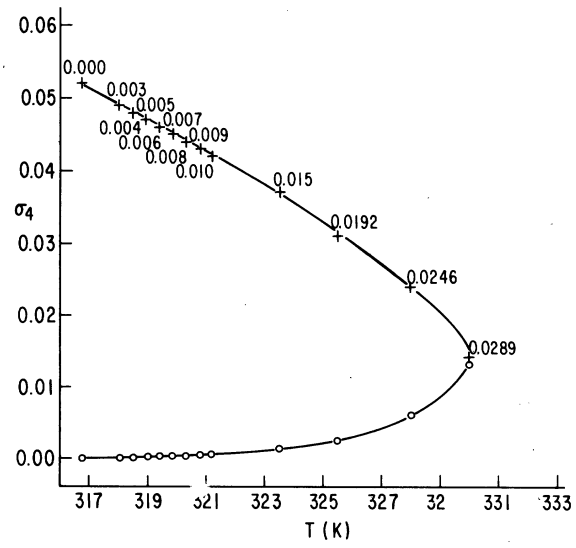

FIG. 2. Coexistence curve: σ_4 at transition temperatures T_{PN}.

not symmetrical with respect to the critical value $\sigma_4 \approx 0.0135$. This is a new discovery. We do not yet have an interpretation for it. It suffices to say at the moment that σ_4 has been known to exhibit strange phenomena. For example, in MBBA it turns negative at temperatures near the clearing point in the absence of an external field.[18-20] There has not been much study done on σ_4. We speculate that these strange phenomena may be related.

Figure 3 expresses the phase diagram in a different form. The transition temperature is seen to be almost linear in ν, both for the Maier-Saupe theory[5] and our present OAPC calculation. Each line terminates on a critical point.

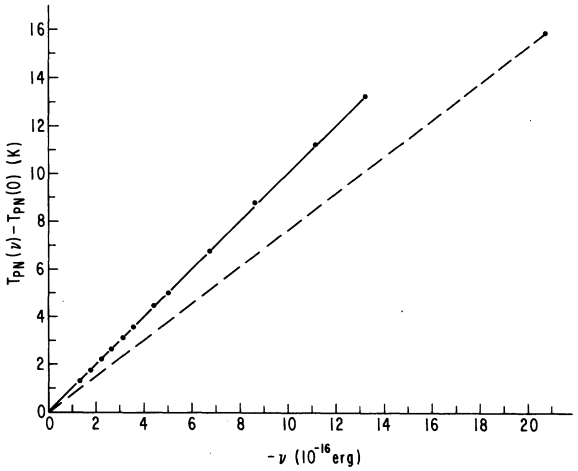

FIG. 3. T-ν phase diagram. Solid curve: present calculation. Dashed curve: Ref. 5.

IV. COMPARISON WITH OTHER THEORIES AND EXPERIMENT

The external field can be magnetic or electric. We look at the two cases separately.

A. Magnetic field

In a magnetic field $\vec{H}$,

$$\nu = \frac{-(\Delta\chi)_{\max} H^2}{3}, \tag{33}$$

where $(\Delta\chi)_{\max}$ denotes the diamagnetic anisotropy $\chi_\parallel - \chi_\perp$, of a single molecule. The results in the previous section can all be interpreted in the light of Eq. (33).

Each of the three figures indicates a critical point at $T_{PN} = 330.1$ K and $\nu_c = -0.029 k T^c_{PN} = -1.32\times10^{-15}$ erg, or a critical magnetic field

$$H_c = [-3\nu_c/(\Delta\chi)_{\max}]^{1/2} = 8.6\times10^6 \text{ G or } 7\times10^6 \text{ G}, \tag{34}$$

depending on the value of $(\Delta\chi)_{\max}$ assumed for MBBA. The fact that we have two answers needs further explanation. In Ref. 2, $\Delta\chi$ was reported as 1.25×10^{-7} erg G^{-2} cm^{-3}. It was used as $(\Delta\chi)_{\max}\rho$. If we follow that practice, H_c obtains the former value. On the other hand, if $\Delta\chi$ is regarded as macroscopic data, as we suspect that it should have been, the relation[20]

$$\Delta\chi = \rho\sigma_2(\Delta\chi)_{\max}$$

would yield[21] $(\Delta\chi)_{\max} = (\Delta\chi)/\sigma_2\rho \approx 8\times10^{-29}$ erg G^{-2} (taking σ_2 as 0.67 at the experimental temperature). H_c would then obtain the latter value. In either case, the critical field is too large to attain. The same conclusion was reached by Wojtowicz and Sheng in Ref. 5 using the Maier-Saupe theory. Note that the Landau–de Gennes theory yields a T^c_{PN} which is less than 1 K above the clearing point, and a critical field of only about 1×10^6 G. We shall return to this point near the end of this paper.

When we deal with the magnetic field, then, only an extremely small portion of the phase diagram (on the left end) is useful. There, our interest is on the Cotton-Mouton coefficient defined as the slope of $H^2/\Delta n$ as a linear function of the temperature, where Δn denotes the magnetically induced birefringence. As shown in Ref. 20,

$$\Delta n = \frac{(\Delta\epsilon)_{\max}}{2\bar{\epsilon}^{1/2}}\sigma_2,$$

where

$$\bar{\epsilon} = \tfrac{1}{3}(\epsilon_\parallel + 2\epsilon_\perp),$$

and

$$\Delta\epsilon = \epsilon_\parallel - \epsilon_\perp = \sigma_2(\Delta\epsilon)_{\max},$$

$\epsilon_\parallel(\epsilon_\perp)$ being the long-wavelength dielectric constant parallel (perpendicular) to $\vec{H}$. As $H\to0$, the induced $\sigma_2\to0$; an expansion of Eq. (27) leads Eq. (22) to

$$\sigma_2 = \frac{-\nu}{\rho\gamma_2 + 5kT} = \frac{\frac{1}{3}(\Delta\chi)_{\max}H^2}{\rho\gamma_2 + 5kT}. \tag{35}$$

Thus,

$$\frac{H^2}{\Delta n} = \frac{30k\bar{\epsilon}^{1/2}}{(\Delta\epsilon)_{\max}(\Delta\chi)_{\max}}\left(T + \frac{\rho\gamma_2}{5k}\right). \tag{36}$$

Taking as in Ref. 2 $\bar{\epsilon} = 2.605$ and $(\Delta\epsilon)_{\max} = 1.09$, the Cotton-Mouton coefficient is determined as

$$C = \frac{30k\bar{\epsilon}^{1/2}}{(\Delta\epsilon)_{\max}(\Delta\chi)_{\max}} = \begin{cases} 1.13\times10^{14}\ \text{G}^2\,\text{K}^{-1} & \text{for } (\Delta\chi)_{\max} = \dfrac{\Delta\chi}{\rho} = 5.4\times10^{-29}\ \text{erg G}^{-2}, \\ 0.75\times10^{14}\ \text{G}^2\,\text{K}^{-1} & \text{for } (\Delta\chi)_{\max} = \dfrac{\Delta\chi}{\sigma_2\rho} = 8\times10^{-29}\ \text{erg G}^{-2}. \end{cases} \tag{37}$$

This is, of course, no different from the result that one obtains using the Maier-Saupe theory. The difference comes in the intercept of $H^2/\Delta n$ on the temperature axis, or the maximum supercooling temperature T^*.

By adopting a Landau–de Gennes interpretation:

$$\frac{H^2}{\Delta n} = C(T - T^*), \tag{38}$$

Eq. (36) identified T^* as $-\rho\gamma_2/5k$, which in the present calculation turns out to be 294 K, or 23 K below the transition temperature, if we use the γ_2 value at the transition temperature. In the Maier-Saupe theory, the corresponding numbers are 288 and 29 K. The fact that the molecular-theoretic values lie so far from the Landau–de Gennes value of $T_{IN} - T^* \sim 1$ K has long been a source of puzzlement. No resolution can be reached as long as we insist on truncating the Landau–de Gennes free energy at the quadratic term in σ_2, which is responsible for Eq. (38). In Ref. 9, we offer a new analysis of the Landau–de Gennes theory which appears to shed some light on a possible resolution of this dilemma. Such a discussion lies outside the scope of our present paper.

There is an alternate way of obtaining T^* which is physically more appealing. Following Ref. 4, we write for small ν:

$$\frac{\sigma_2}{\nu} = \left(\frac{\partial\sigma_2}{\partial\nu}\right)_{\nu=0} + \frac{1}{2}\left(\frac{\partial^2\sigma_2}{\partial\nu^2}\right)_{\nu=0}\nu + \cdots . \tag{39}$$

Taking σ_2/ν from the paranematic entries in Table I and plotting it against ν for varying temperatures, we obtain a set of curves whose intercepts give us $(\partial\sigma_2/\partial\nu)_{\nu=0}$ and whose slopes at small ν give us $\frac{1}{2}(\partial^2\sigma_2/\partial\nu^2)_{\nu=0}$. Plotting next the reciprocals of $(\partial\sigma_2/\partial\nu)_{\nu=0}$ against the temperature, the intercept on the temperature axis gives us T^*. Furthermore, plotting

$$f \equiv \frac{1}{2}\left(\frac{\partial^2\sigma_2}{\partial\nu^2}\right)_{\nu=0}\nu \Big/ \left(\frac{\partial\sigma}{\partial\nu}\right)_{\nu=0} \tag{40}$$

against $(T - T^*)$ on a log-log scale yields a slope Δ which is a critical exponent. In the Landau–de Gennes framework Δ distinguishes tricritical behavior ($\Delta = \frac{5}{4}$) from mean-field behavior ($\Delta = 2$).[4]

We have attempted to follow the procedure outlined above to obtain T^* and Δ. Unfortunately, the range of our ν values is too far from $\nu = 0$ to allow for meaningful extrapolations, and numerical accuracy does not permit us to seek solutions for smaller ν. It is far better to alter the procedure slightly, as follows.

By differentiating Eq. (22) with respect to ν, we find

$$\left(\frac{\partial\sigma_2}{\partial\nu}\right)_{\nu=0} = \frac{-1}{5kT + \rho\gamma_2(\nu=0, T)} = \frac{-1}{5k}\,\frac{1}{\left(T + \dfrac{\rho\gamma_2(\nu=0, T)}{5k}\right)} . \tag{41}$$

Table III lists $\gamma_2(\nu=0, T)$ and $(\partial\sigma_2/\partial\nu)_{\nu=0}$, and lists a few values of the latter as extrapolated from plotting σ_2/ν versus ν for comparison. Plotting the reciprocal of $(\partial\sigma_2/\partial\nu)_{\nu=0}$ against temperature and extrapolating yields the intercept T^*, which

TABLE III. Data for determination of the maximum supercooling temperature.

T(K)	$\frac{-\rho\gamma_2(\nu=0,T)}{5k}$	$-k\left(\frac{\partial\sigma_2}{\partial\nu}\right)_{\nu=0}$ (K^{-1}) From Eq. (41)	From plotting σ_2/ν vs ν
314.4	293.55	0.009 591	
315.4	293.63	0.009 187	
316.4	293.70	0.008 811	
317.4	293.77	0.008 464	0.0084
318.4	293.81	0.008 135	0.0081
319.4	293.88	0.007 838	0.0078
320.4	293.95	0.007 560	0.0074
321.4	294.01	0.007 303	0.0070
322.5	294.12	0.007 048	
323.5	294.19	0.006 824	
324.5	294.26	0.006 614	
325.5	294.33	0.006 417	
326.5	294.40	0.006 231	
328.0	294.50	0.005 970	
329.0	294.57	0.005 809	
330.0	294.64	0.005 656	

turns out to be 292 K.

Differentiating Eq. (22) twice with respect to ν gives us:

$$\left(\frac{\partial^2\sigma_2}{\partial\nu^2}\right)_{\nu=0} = \frac{2}{35k^2}\,\frac{T}{\left(T+\frac{\rho\gamma_2(\nu=0,T)}{5k}\right)^3}\,. \tag{42}$$

From Eqs. (40)–(42) and the identification of T^* as $-\rho\gamma_2/5k$, we obtain

$$f(T-T^*) = \frac{1}{7}\left(\frac{-\nu}{kT}\right)\frac{T^2}{(T-T^*)^2}\,. \tag{43}$$

The critical behavior, given here as $\Delta=2$, is still mean field. This is not unexpected since OAPC treats the orientational order in a mean-fieldlike manner. In order to find a molecular-theoretic basis for the data reported in Ref. 5, we will need to go beyond OAPC, and quite possibly beyond the present potential model as well. Both directions are at present under exploration in our group. See, for example, Ref. 11.

B. Electric field

In an oscillating electric field,

$$\nu = \frac{-\Delta\alpha}{6}\,\frac{\epsilon(\epsilon+2)}{2\epsilon+1}\,\langle E^2\rangle_{\rm av}\,, \tag{44}$$

where $\Delta\alpha \equiv \alpha_{\parallel} - \alpha_{\perp}$ denotes the single-molecule polarizability anisotropy and $\langle E^2\rangle_{\rm av}$ is the time-averaged value of E^2. This result comes from considering the orientational energy of a single molecule in a field $\vec{F}$ that includes the cavity field and the reaction field. Following Ref. 6, we find first of all:

$$\vec{F} = \frac{3\epsilon}{2\epsilon+1}\,\vec{E} + \frac{2(\epsilon-1)}{2\epsilon+1}\,\frac{\vec{p}}{a^3}\,, \tag{45}$$

where a is the radius of the cavity that contains the molecule. Let β_i stand for the direction cosines of $\vec{E}$ in the molecular axis coordinate system. The polarization vector appears as

$$p_i \equiv \alpha_i'\beta_i E = \frac{3\epsilon}{2\epsilon+1}\,\alpha_i\beta_i E + \frac{2(\epsilon-1)}{(2\epsilon+1)a^3}\,\alpha_i p_i\,. \tag{46}$$

Thus,

$$\alpha_i' = \frac{3\epsilon a^3\alpha_i}{(2\epsilon+1)a^3 - 2(\epsilon-1)\alpha_i}\,. \tag{47}$$

Under cylindrical symmetry, $\alpha_1' = \alpha_2' \equiv \alpha_{\perp}'$ and $\alpha_3' = \alpha_{\parallel}'$. Let

$$\bar{\alpha} = \tfrac{1}{3}(2\alpha_{\perp}' + \alpha_{\parallel}')\,, \tag{48}$$

and take from Lorentz's formulation of the local field

$$\bar{\alpha} = \frac{\epsilon-1}{\epsilon+2}\,a^3\,. \tag{49}$$

With the help of these relations we reduce Eq. (47) to the following simple form by approximating α_i by $\bar{\alpha}$ in its denominator:

$$\alpha_i' = \frac{\epsilon+2}{3}\,\alpha_i\,. \tag{50}$$

Now, the orientational energy V_Ω is given by $-\frac{1}{2}\vec{E}_{\rm cav}\cdot\vec{p}$. The field inside the cavity $\vec{E}_{\rm cav}$ can be determined from solving the Laplace equation and matching boundary conditions. It is the first term in Eq. (45):

$$\vec{E}_{\rm cav} = \frac{3\epsilon}{2\epsilon+1}\,\vec{E}\,. \tag{51}$$

Thus

$$V_\Omega = -\frac{1}{2}\,\frac{3\epsilon}{2\epsilon+1}\sum_i \alpha_i'\beta_i^2 E^2 = -\frac{1}{4}\,\frac{3\epsilon}{2\epsilon+1}\,\langle E^2\rangle_{\rm av}(\alpha_{\parallel}'\cos^2\theta + \alpha_{\perp}'\sin^2\theta)\,, \tag{52}$$

where θ is the angle between $\vec{E}$ and the molecular axis. Using Eq. (50) and omitting terms not dependent upon the orientation we obtain

$$V_\Omega = -\frac{\epsilon}{2\epsilon+1}\,\frac{\langle E^2\rangle_{\rm av}}{2}\,\Delta\alpha' P_2(\cos\theta) = -\frac{1}{6}\,\frac{\epsilon(\epsilon+2)}{2\epsilon+1}\,\Delta\alpha\langle E^2\rangle_{\rm av}P_2(\cos\theta)\,; \tag{53}$$

thus the result in Eq. (44).

We can now interpret our results in the light of Eq. (44). Taking ϵ as $\bar{\epsilon}=2.605$, and

$$\Delta\alpha = \frac{1}{4\pi\rho}\,(\Delta\epsilon)_{\rm max}\,, \tag{54}$$

with $\rho = 0.002\,315$ Å^{-3} and $(\Delta\epsilon)_{\rm max} = 1.09$ as before, we obtain the numerical results shown in Table IV. The last column gives the root-mean-square electric field required to induce a transition at the temperature $T_{PN}(E)$ shown in the second column. To reach the critical temperature 330.1 K, which is about 13 K above our constant-volume transition temperature 316.74 K, our theory indicates the requirement of a field strength of approximately 10^4 esu. We understand that this is not very demanding: Such field strengths can be readily obtained by focusing a 100-kW laser beam into a 50-μm spot.[8] So optical-field-induced I-N transitions should be observable throughout the phase diagram. In particular, one should be able to see the critical point, which is so far outside the range of experimental capability in the magnetic case but well within reach with a laser beam.

TABLE IV. Transition temperature and root-mean-square electric field.

$-\nu/kT$	$T_{PN}(E)-T_{PN}(0)$ (K)	$\langle E^2\rangle_{av}(10^8$ esu)	$E_{rms}(10^4$ esu)
0.0000	0.00	0.0000	0.000
0.0030	1.32	0.1092	0.330
0.0040	1.76	0.1459	0.382
0.0050	2.21	0.1827	0.427
0.0060	2.66	0.2195	0.469
0.0070	3.12	0.2565	0.506
0.0080	3.57	0.2935	0.542
0.0090	4.03	0.3307	0.575
0.0100	4.48	0.3679	0.607
0.0150	6.76	0.5558	0.746
0.0192	8.76	0.7158	0.846
0.0246	11.26	0.9242	0.961
0.0289	13.26	1.0924	1.045

It was called to our attention by Wong[8] that our analysis depends on two conditions. First, since we used equilibrium statistical mechanics in our analysis, the laser pulse used must have duration which is long compared to the molecular reorientation time. Next, since we dealt with the *constant-volume* transition temperature, the pulse should be short compared to the time required for macroscopic volume adjustment. Wong further pointed out that these two conditions could readily be met with laser pulses for a few μsec duration.[8] (The molecular reorientation time for MBBA is of the order of 100 nsec.[7]) In fact, for experiments with electric fields (laser beams), our use of the *Helmholtz* free energy turned out to be entirely appropriate.

Our results are very different from that of the Landau–de Gennes theory, as was pointed out earlier in this section. Let us review very briefly the latter analysis.

The free energy is expanded in a power series in the order parameter σ_2, thus,

$$\mathfrak{F}=F_0+a(T-T^*)\sigma_2^2+B\sigma_2^3+C\sigma_2^4+\nu\sigma_2, \tag{55}$$

where a, B, C, and T^* are parameters to be determined from zero-field experimental data including the I-N transition temperature $T_{IN}\equiv T_{PN}(\nu=0)$, the order parameter at that temperature $\sigma_2(T_{IN})$, the latent heat, and light scattering data. Such an analysis depends much more heavily on empirical information than our molecular theory. The relation between the two approaches, in particular that between the free-energy functionals (55) and (9), will be examined in detail in Ref. 9.

Possible states of equilibrium occur at the solutions of the equation

$$0=\frac{\partial\mathfrak{F}}{\partial\sigma_2}=\nu+2a(T-T^*)\sigma_2+3B\sigma_2^2+4C\sigma_2^3. \tag{56}$$

For every set of the thermodynamic variables (T,ν), there will be up to three real solutions. $T_{PN}(\nu)$ is given by the temperature at which the two solutions that produce minima give rise to equal values of $\mathfrak{F}$. This yields a T-ν phase diagram: a coexistence curve. Since eventually at some T_{PN}^c and ν_c the two minima will coincide, the curve will terminate on a critical point. In fact, at that point all three solutions will coincide. Simple algebra shows that

$$T_{PN}^c=\frac{3B^2}{8aC}+T^*, \tag{57}$$

and

$$\nu_c=\frac{B^3}{16C^2}. \tag{58}$$

Using the values $a=0.0315$ J/cm^{3}K, $B=-0.160$ J/cm^3, $C=0.197$ J/cm^3, and $T^*=T_{IN}-1$ K, as given in Ref. 1 (beware of the difference in the definitions of a, B, and C), we find

$$T_{PN}^c=T_{IN}+0.55\ \text{K},\qquad \nu_c=-0.0066\ \text{J/cm}^3\ \text{or}\ -2.85\times10^{-17}\ \text{erg per molecule}. \tag{59}$$

Using more recent values[9]: $a=0.0265$ J/cm^{3}K, $B=-0.170$ J/cm^3, $C=0.272$ J/cm^3, and $T^*=T_{IN}-1$ K (again note the difference in the definitions of a, B, and C), we find

$$T_{PN}^c=T_{IN}+0.50\ \text{K},\qquad \nu_c=-0.0042\ \text{J/cm}^3\ \text{or}\ -1.81\times10^{-17}\ \text{erg per molecule}. \tag{60}$$

In either case, T_{PN}^c lies only about half a degree above the zero-field clearing point, while ν_c lies nearly two orders of magnitude lower than that calculated in the molecular theory. This means that H_c is an order of magnitude lower: about 1×10^6 G, and likewise E_{rms}: about 10^3 esu.

The critical magnetic field becomes possibly attainable.[22] The critical electric field is certainly well within reach.

The discrepancy between results from the Landau–de Gennes theory and our present molecular theory comes from many sources. The first problem, in our opinion, is the inadequate treatment of order-parameter fluctuations in the Gaussian approximation, i.e., in omitting B and C in Eq. (55), as employed in the Landau–de Gennes model. This leads to errors in T^*, and subsequently the equilibrium values of B and C, by as much as an order of magnitude.[9] In the present problem, the Landau–de Gennes model further neglects the ν dependence of the parameters, which has highly nonlinear effects and may become rather dominant when the fields approach the critical region.

We understand that there are experimental indications of laser-induced transitions, but the data are not yet conclusive.[8] Such experiments are well worth pursuing, partly because they will help solve some of the puzzles that occur in the fundamental structure of the theory of liquid crystals, and partly because of obvious possibilities of technical applications.

ACKNOWLEDGMENTS

This work is supported in part by the U. S. National Science Foundation through Grant No. DMR80-08816, and in part by the Chinese Academy of Sciences. We are indebted to Dr. L. Lin (Institute of Physics, China), Dr. L. Senbetu (University of California, San Diego), Dr. G. Wong (Northwestern), and Dr. P. Sheng (Exxon) for valuable and stimulating discussions.

---

*Permanent address of Chia-Wei Woo.

†Permanent address of Juelian Shen.

[1]For a quick review, see E. B. Priestley, P. J. Wojtowicz, and P. Sheng, in *Introduction to Liquid Crystals* (Plenum, New York, 1975), Chap. 10.

[2]T. W. Stinson and J. D. Litster, Phys. Rev. Lett. 25, 503 (1970).

[3]Y. Poggi, P. Atten, and R. Aleonard, Phys. Rev. A 14, 466 (1976).

[4]P. H. Keyes and J. R. Shane, Phys. Rev. Lett. 42, 722 (1979).

[5]P. J. Wojtowicz and P. Sheng, Phys. Lett. 48A, 235 (1974).

[6]J. Hanus, Phys. Rev. 178, 420 (1969).

[7]G. Wong and Y. R. Shen, Phys. Rev. A 10, 1277 (1974).

[8]Y. M. Shih and G. Wong (private communications).

[9]L. Senbetu and C.-W. Woo (unpublished).

[10]L. Senbetu and C.-W. Woo, Phys. Rev. A 17, 1529 (1978).

[11]J. Shen, L. Lin, L. Yu, and C.-W. Woo, Mol. Cryst. Liq. Cryst. (in press).

[12]S. Chakravarty and C.-W. Woo, Phys. Rev. A 11, 713 (1975); A 12, 245 (1975).

[13]Y. M. Shih, Y. R. Lin-Liu, and C.-W. Woo, Phys. Rev. A 14, 1895 (1976).

[14]Y. M. Shih, H. M. Huang, and C.-W. Woo, Mol. Cryst. Liq. Cryst. (Lett.) 34, 7 (1976).

[15]M. A. Lee and C.-W. Woo, Phys. Rev. A 16, 750 (1977).

[16]V. T. Rajan and C.-W. Woo, Phys. Rev. A 17, 382 (1978).

[17]L. Feijoo, V. T. Rajan, and C.-W. Woo, Phys. Rev. A 19, 1263 (1979).

[18]S. Jen, N. A. Clark, P. S. Perhsan, and E. B. Priestley, Phys. Rev. Lett. 31, 1552 (1973).

[19]K. Miyano, Phys. Lett. 63A, 37 (1977).

[20]See, for example, discussions in E. B. Priestley, P. J. Wojtowicz, and P. Sheng, in *Introduction to Liquid Crystals* (Plenum, New York, 1975), Chaps. 4 and 6.

[21]J. G. Ypma and G. Vertogen, J. Phys. (Paris) 37, 557 (1976).

[22]N. Miura, G. Kido, M. Akihiro, and C. Chikazumi, J. Magn. Mater. 11, 275 (1979).